An Empirical HBT Large-Signal Model for CAD

I. Angelov,[1] K. Choumei,[2] A. Inoue[2]

[1] Microwave Electronics Laboratory, Chalmers University of Technology, S-41296 Göteborg, Sweden
[2] Mitsubishi Electric Corporation, 4-1 Mizuhara Itami Hyogo, Japan

Received 10 October 2002; accepted 19 June 2003

ABSTRACT: A new, simple heterojunction bipolar transistor (HBT) large-signal model for use in CAD is proposed and experimentally evaluated. The important development in this model is that the main model parameters are derived directly from the measurements taken during typical operating conditions. The model was evaluated with extensive measurements at different temperatures by DC, *S*, and power-spectrum measurements. Good correspondence was obtained between the measurement and experimental results. © 2003 Wiley Periodicals, Inc. Int J RF and Microwave CAE 13: 518–533, 2003.

Keywords: nonlinear models for active devices; nonlinear circuit design; microwave circuits

I. INTRODUCTION

Heterojunction bipolar transistors (HBTs) have become very promising devices for different applications at microwave and millimeter-wave frequencies. An important condition for any successful design is the availability of an accurate large-signal model (LSM). In recent years, more than 100 papers in the literature have been devoted on the creation of a compact model for use in CAD tools and procedures for extraction of parameters for these models [1–29]. Despite the tremendous work already done on the subject, we still do not have unified, accurate model standards in the industry, together with an automatic extraction procedure. The reason for this is that the physics of the device is very complicated, the range of currents is broad, and the power density at which the device operates is very high. All this, together with poor thermal conductivity of the III-V materials, makes the problem of creating universal LSM for HBTs difficult. Many of the existing HBT models are based on solid physical background, but again, because of the difficulties of the problem, they end up with many empirical coefficients that are difficult to extract.

In some cases, the HBT models can be excessively accurate and include effects that may not be particularly important; model simplification is appropriate in such cases. When the model is complicated, an additional difficulty is added to the extraction problems — such a model may exhibit problems with convergence.

II. DEVICE MODELING

The HBTs used in this study are mainly AlGaAs/GaAs HBTs with a $4 \times 20\ \mu m^2$ emitter [30]. Systematic DC and multi-bias *S*-parameter measurements were performed at different temperatures (−25–+125°C) in order to obtain a general picture of the device's behavior. ICCAP software (Agilent) was used in the measurement and extraction of basic parasitic parameters such as parasitic resistances, parasitic capacitances, and bias dependencies of C_{be} and C_{bc}.

The frequency range of the *S*-parameter measurements were determined by the frequency range in which the devices should operate and the available measurement setup.

Correspondence to: I. Angelov; email: angelov@ep.chalmers.se
Published online in Wiley InterScience (www.interscience.wiley.com). DOI 10.1002/mmce.10110

© 2003 Wiley Periodicals, Inc.

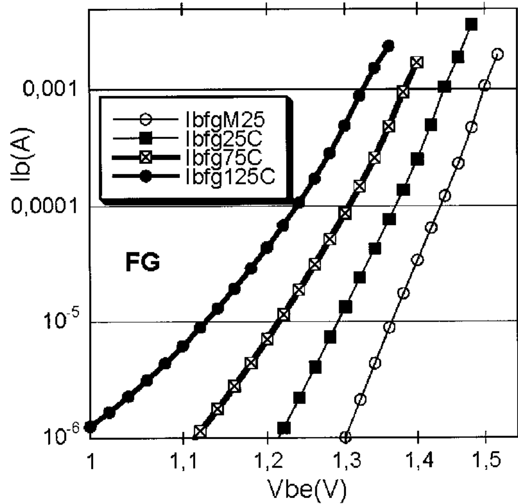

Figure 1. I_{be} FG.

Figures 1–3 show some results for the forward Gummel (FG) I_{be}, I_{ce}, and β obtained from these devices that are typical of many HBTs. As can be seen in Figure 4, when keeping the I_{be} (or I_{ce}) constant, the voltage shift of the BE junction is almost linear and can be used to monitor the device's temperature. Increasing the temperature will decrease the base voltage required to sustain the same current and the temperature coefficient is rather small, with $T_c V_{jbe} \sim -0.002$. A problem with this type of transistors is that β cannot be considered constant (see Fig. 3). The models that consider β constant, such as the Gummel–Poon model, produce significant error, and separate equations for I_{be} and I_{ce} should be used in this model. In addition, it should be considered that there is a bias dependence of the voltage $V_{be} = f(V_{ce})$ at which we have maximum of β. At the change of the

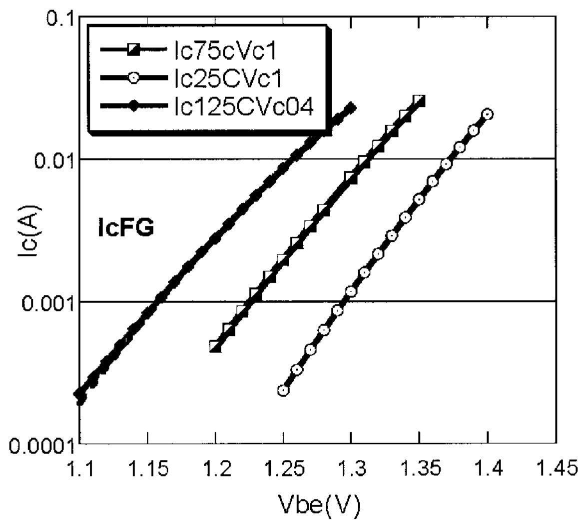

Figure 2. I_{ce} vs. V_{be}.

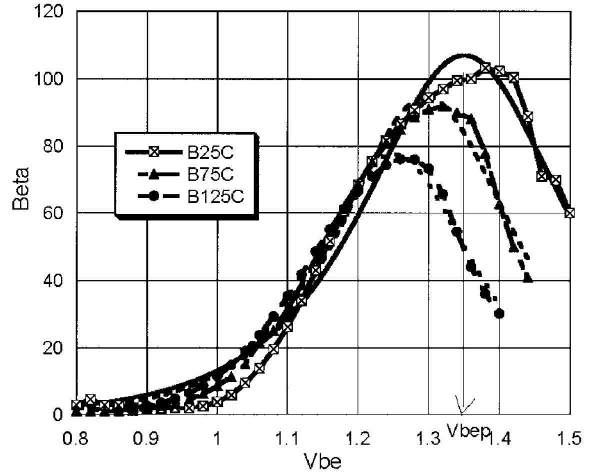

Figure 3. FG β vs. V_{be} & T.

V_{be}, we have maximum β and this needs to be considered in the LSM. The logogriphic plots in Figures 1 and 2 are close to a straight line (as should be the case based on the device physics), but deviate at small currents. This means that the main function describing the device current should be exponential with a proper correction.

The transistor can be described with a conventional equivalent circuit shown in Figure 6. Current source I_{ce} with transconductance g_m is nonlinear, and also nonlinear can be considered capacitances C_{be} and C_{bc}. The remaining elements can be considered linear and there is a significant amount of papers that describing extraction of the small-signal equivalent circuit [14–28]. For devices exhibiting substrate effects, an extra port should be added.

Base Current

We can significantly simply the self-heating modeling if we use the fact that, when keeping the diode current

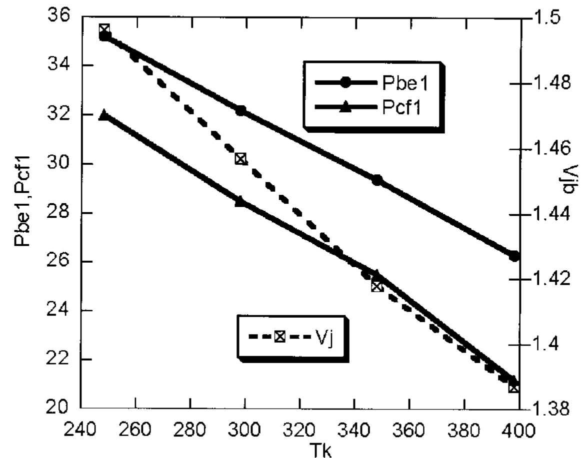

Figure 4. $Vjbe$, $Pbe1$, $Pcf1$ vs. T.

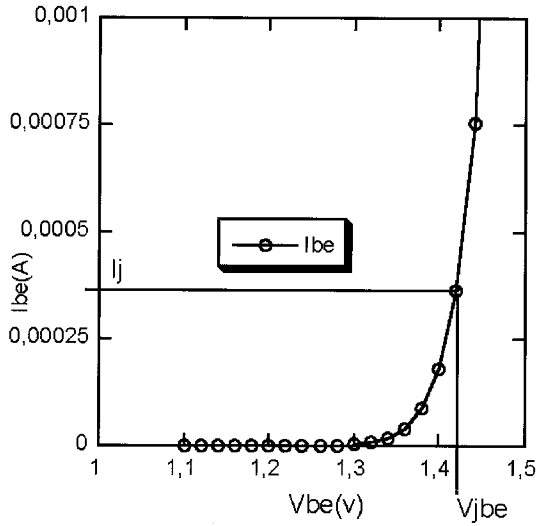

Figure 5. I_{be} vs. V_{be}.

constant, the junction voltages vary linearly with the temperature; however, this requires modification of the diode-current definition. It is a common practice to describe the complicated I_{be} dependence by several diodes (respective exponential functions) in order to improve the accuracy and describe the different physical phenomena occurring in the device [1–12]. According to the device physics, we use an exponential function to describe the semiconductor junction, but change the reference points of the currents and respective voltages at which we normally operate the device to be closer to the currents (voltages) at which β is maximum (see Fig. 3). In addition to this change of reference points, the argument of the equation for the junction current is described as a power series. This gives us the possibility to fit a variety of doping profiles; many factors and effects will influence the currents:

$$I_b = I_{be} + I_{bc}$$

$$I_{be} = I_{jbe}(\exp(P_{be}) - \exp(P_{be0})), \quad (1)$$

$$I_{bc} = I_{jbc}(\exp(P_{bc}) - \exp(P_{bc0}), \quad (2)$$

$$P_{be} = P_{be1}(V_{be} - V_{je}) + P_{be2}(V_{be} - V_{je})^2 \ldots, \quad (3)$$

$$P_{be0} = -P_{be1} \cdot V_{je} - P_{be2} \cdot V_{je}^2 \ldots,$$

$$P_{bc} = P_{bc1}(V_{bc} - V_{jc}) + P_{bc2}(V_{bc} - V_{jc})^2 \ldots$$

$$P_{bc0} = P_{bc1} \cdot (-V_{jc}) + P_{bc2} \cdot (-V_{jc}^2) \ldots, \quad (4)$$

$$P_{be1} = q_e/K_b \cdot T_{ambK} \cdot N_{b1} = 1/V_t \cdot N_{e1} \cong 38.695/N_{b1}, \quad (4a)$$

where q_e- is the electron charge, K_b- is the Boltzmann constant, and N_{b1} is the ideality factor. The coefficient 38.695 $\cong$ $1/V_t$ at room temperature.

This definition is equivalent to a conventional diode equation, but the extraction point is changed. In a textbook definition of the diode current, the extraction point in fact is at $V_{be} = -\infty$. At small currents, the measurement data are quite often noisy and, what is most important, we usually do not operate the device at such small currents. With the reference and extraction points selected in the operating region of voltages and currents, we will describes the currents with highest accuracy in the useful operating range.

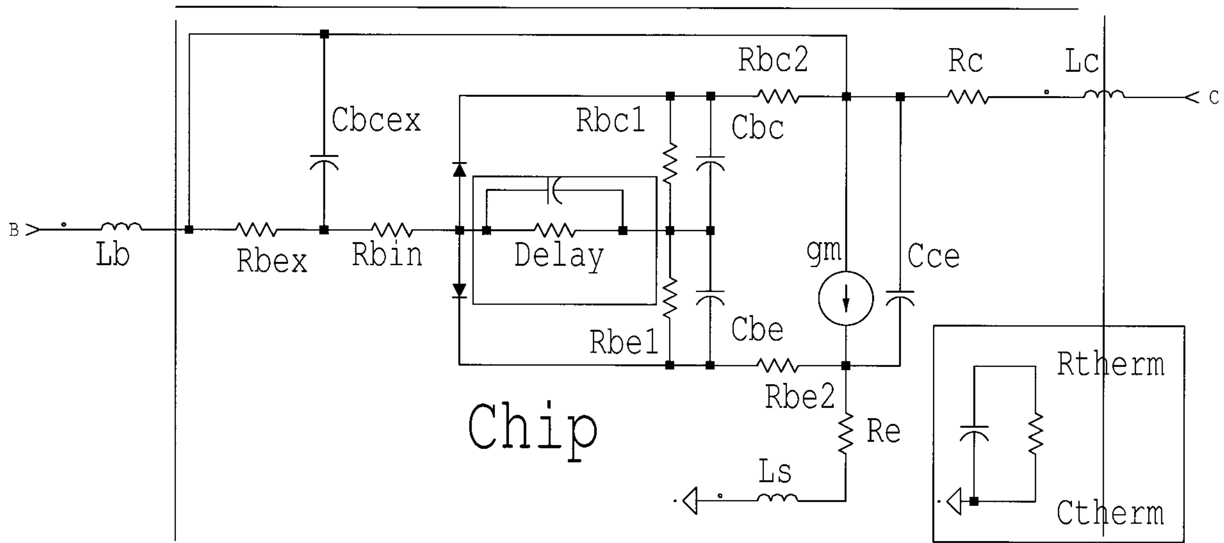

Figure 6. Transistor equivalent circuit.

TABLE I.

Current parameters								
I_{pkc} (mA)	N_{cf1}	N_{cf2}	V_{bep} (V)	α_r	α_s	λ	β	B_{be}
25.0	1.3	0	1.39	0.3	0.15	0.035	105	6
I_{jb} (mA)	N_{be1}	N_{be2}	V_{jbe}	D_{vpk}	—	—	—	—
0.24	1.2	0	1.39	0.01	—	—	—	—
Parasitics								
R_e	R_c	R_{bmin}	R_{max}	R_{bex}	R_{bc1}	n	m	Vc_{min}
1.3	1.4	4	4.1	4.2	4	0.5	0.05	2.1
C_{bep}	C_{be0}	C_{bcp}	C_{bc0}	C_{P10}	C_{P11}	C_{P20}	C_{P21}	—
5 ff	350 ff	6 ff	33	1.1	1.04	0.1	0.5	—
Temperature coefficients								
T_cI_{pkc}		T_cV_j		$T_c\beta$		$T_cC_{be}0$		$T_cC_{bc}0$
0.002		−0.0018		−0.008		+0.001		0.001

When $V_{be} = V_{je}$, the base current I_{be} is equal to I_{jbe} and when $V_{be} = 0$, $I_{be} = 0$. The terms P_{be0}, P_{bc0} are important to define the current to be zero when the voltage at the junction is zero. The correction is small, but critical so that the HB will converge properly. The equations for P_{be0} and P_{bc0} are obtained by substituting in equations for P_{be}, P_{bc}, $V_{be} = 0$, and $V_{bc} = 0$, respectively. Usually, one term in the power series is enough to provide accuracy of better then 5% in five-to-six decades of the diode current. If higher accuracy is required, or for some reason is important to keep this accuracy in a range of currents more then six decades, then more terms can be used. Typically, three terms of the power series are enough to obtain 2% global accuracy.

The approach of using power series in the argument is equivalent to fitting the specific doping profile of the device which will determine currents I_{be} and I_{ce}. Using this approach, we can reduce the number of the diodes (exponents) and obtain very high accuracy. The reduction of the number of exponents in turn will improve the convergence of the LSM.

The temperature dependence of I_{be}, I_c, β versus V_{be} is one of the main factors responsible for the high temperature sensitivity of these devices. Figure 4 and Table I show extracted parameters of the base part of the model, using one term in the power series of eqs. (1–3) at different temperatures. The changes of the parameters are almost linear with respect the temperature and this can be used to model self-heating in a simple way by using linear dependencies. In fact, the current of the bipolar devices is controlled by the intrinsic diode voltage, but when the device is biased with a constant DC voltage source at the base, this can produce a thermal runaway; the model should describe this phenomenon.

Collector Current

In a method similar to that used with the base current, we can keep the basic form of the Gummel–Poon model [10], but shift the reference point at V_{bep} and define the collector current source argument as a power series:

$$I_c = I_{pkc}(\exp(P_{cf}) - \exp(P_{cr}))\left(1 - \frac{V_{be}}{V_{ar}} - \frac{V_{bc}}{V_{af}}\right), \quad (5)$$

where P_{cf} is a power series centered at V_{pcs} and with a variable V_{be}, given by

$$\begin{aligned} P_{cf} &= P_{cf1}(V_{be} - V_{bepm}) + P_{cf2}(V_{be} - V_{bepm})^2 \ldots \\ P_{cf0} &= P_{cf1}(-V_{bepm}) + P_{cf2}(-V_{bepm})^2 \ldots \\ P_{cr} &= P_{cr1}(V_{bc} - V_{bcpm}) + P_{cr2}(V_{bc} - V_{bcpm})^2 \ldots \\ P_{cr0} &= P_{cr1}(-V_{bcpm}) + P_{cr2}(-V_{bcpm})^2 \ldots g_m \\ &= \frac{q}{\eta K_b T} I_{cf}. \end{aligned} \quad (6)$$

When $V_{be} = V_{bep}$, the collector current is equal to I_{pkc}, the transconductance is equal to $g_m = I_{pkc} \cdot P_{cf1}$.

The V_{bep} and I_{pkc} are taken directly from the measurements and there is some freedom for their selection. Probably, the best choice is to select V_{bep} equal to the voltage at which $\boldsymbol{\beta}$ is maximum, but usually even a simple fitting program will converge and find the optimum values, because of the presence of an

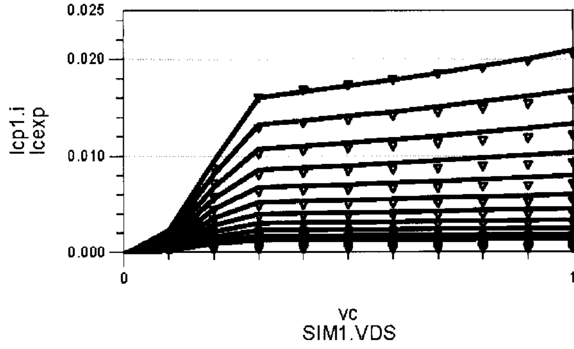

Figure 7. Measured and modeled I_{ce} vs. V_{ce} at small V_{ce}.

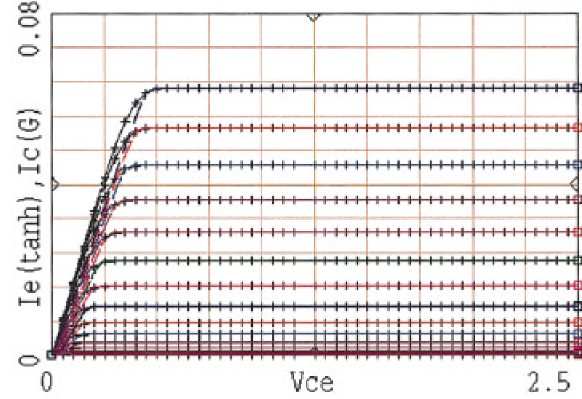

Figure 8. Comparison between the results from eqs. (5) and (7). [Color figure can be viewed in the online issue, which is available at www.interscience.wiley.com.]

inflection point. Typical parameters are I_{be} = 0.2–2 mA and $I_{pkc} \approx I_{ce}$ (at $\beta_{\max}$) with corresponding V_{bep}.

Usually, the device is biased at positive V_{ce}, the forward and reverse part can be considered equal, and these will simply further the equations. The collector current Ice can be expressed in compact form:

$$I_c = I_{cf} \cdot \tanh(\alpha \cdot V_{ce})(1 + \lambda \cdot V_{cb})$$
$$I_{cf} = I_{pkc}(\exp(P_{cf}) - \exp(P_{cf0}))/\cosh(B_{be}(V_{be} - V_{bepm})) \quad (7a)$$

In the case of one term in the power series the arguments P_{cf}, P_{cf0} are transformed to :

$$P_{cf} = P_{cf1}(V_{be} - V_{bepm});\ P_{cf0} = P_{cf1}(-V_{bepm})$$

Some of the parameters like α and V_{bep} are bias dependent due to the Kirk effect, and this should be accounted for as follows:

$$\alpha = \alpha_r + \alpha_s\left(\exp\left(\frac{38.695}{N_{c1}} \cdot V_{ce}\right) - 1\right); \quad (7b)$$

$$V_{bepm} = V_{bep} + \Delta V_{pk} * (1 + \tanh(P_{cf1} * V_{ce}) - V_{sb2} * (V_{cb} - V_{tr})^2; \quad (7c)$$

The parameters α_r, α_s reflect the dependence of the collector current versus V_{be} at small collector voltages, as Figure 7 and parameter B_{be} in the term $1/\cosh(B_{be}\ (V_{ce} - V_{be}\text{pm}))$ will predefine the bell shape of β dependence versus V_{be}. Parameters $\boldsymbol{\alpha}_r$ and $\boldsymbol{\alpha}_s$ adjust precisely the slope at small collector voltages due to the Kirk effect and λ, the output conductance dependence at high V_{ce} due to the Early effect. Parameter V_{sb2} is used in the breakdown modeling.

The definition of I_{ce} behaves well with eq. (7) from a numerical point of view; it converges better than eq. (5), because ***tanh*** is a limited function, with the strictly defined solution I_{ce} = 0 when V_{ce} = 0. In addition, the result will not depend on the correct choice of the forward and reverse parameters of the Gummel-type model.

Figure 8 shows a comparison between the calculated results for the collector current using eqs. (5) and (7). In this figure, for the sake of simplification, one term in the power series was used. As can be seen, the results are almost identical. The model, given by eq. (7), is simpler, with only eight parameters taken directly from measurements. Thus, we can describe the collector current with a good accuracy.

Bounded Current Models for I_{be} and I_{ce}

It is a common practice to limit the exponential growth of the current using a modified exponent (soft exponent). Above some certain value of the exponent, the exponential dependence is switched to a linear dependence and numerical overflow is avoided. But this does not completely solve the problem, because at the connecting point the derivatives will be different and this discontinuity will increase the simulation time.

Taking the approach of using a power series in the argument, we are no longer required to use the soft exponent, because we can limit the exponential growth of the current by selecting the coefficients of the arguments of eq. (3) in a proper way. The derivatives of I_{be} and I_{ce} will not be influenced, because we retain the exponential envelope.

When using a power series in eqs. (1) and (7), the argument function shown in Figure 9 can be adjusted to track the individual properties of the device and behave monotonically from $-\infty$ to $>+\infty$, but we can limit the argument to a useful range.

We can tailor the argument by properly selecting the coefficients to be fitted. For example, when the

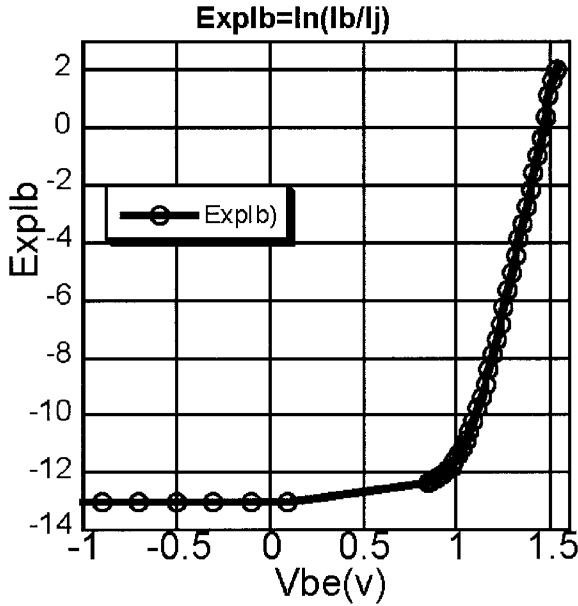

Figure 9. Extracted argument of P_{be} from eq. (3).

second term P_{be2} is used, we should always add a positive 3rd term, P_{be3}, in order to provide stable solution from $-\infty$ to $+\infty$. Fitting of the extracted argument is rather easy, because a polynomial function is used for this purpose.

As shown in Figure 9, the magnitude of the extracted argument is determined by the leakage and the maximum current which the devices can handle (usually not higher then 100 Å). This means that it is possible to use a bounded function to limit the argument, which is important when working with exponential functions as in the case of BT. Simultaneously, it is important to keep a correct value of P_{be1}, because this will determine the derivative (transconductance).

We can use tanh as a limiting function and split the P_{be1} into two parts, $P_{be1\text{e}}$ and $P_{be1\text{i}}$ [see eq. (3a)]. For large deviation from the V_j tanh = 1, $P_{be1\text{e}}$ will determine the maximum of the argument, respective leakage, and the maximum current.

The derivatives will be correct if $P_{be1\text{i}}$ is calculated from:

$$P_{be1} = P_{be1e}\tanh(P_{be1i}).$$

The external parameter $P_{be1\text{e}}$ can be calculated as:

$$\begin{aligned}
P_{be1e} &= ln(I_{be1}/I_{jbe}) \\
P_{be} &= P_{be1e}\cdot\tanh(P_{be1i} * (V_{be} - V_{je}) \\
&\quad + P_{be2}(V_{be} - V_{je})^2 \ldots, \\
P_{be0} &= P_{be1}\cdot\tanh(P_{be1i} * (-V_{je}) \\
&\quad + P_{be2}(-Vje)^2 \ldots) \\
P_{bc} &= P_{bc1}\cdot\tanh((P_{bc1i} * (V_{bc} - V_{jc}) \\
&\quad + P_{bc2}(V_{bc} - V_{jc})^2 \ldots), \\
P_{be0} &= P_{bc1}\cdot\tanh((P_{bc1i} * (-V_{jc}) \\
&\quad + P_{bc2}(-V_{jc})^2 \ldots)
\end{aligned} \tag{3a}$$

The leakage typically is in the order of $I = 10^{-9}$, but usually we do not operate the device at such a small currents. If we fix the magnitude of the exponent, as for example in eq. (3a), to $P_{be} = 1/2V_t \cdot N_{b1} = 19.347/N_{b1}$, this will bound the maximum possible current to $I_{bmax} \sim 126260$ Å and the minimum current to $I_{bmin} \sim 10^{-13}$, which are adequate for most practical cases. If required, the bounding level can be changed. Rewriting the current equations using the ideality factors N_b and N_c leads to the following equations for the base and collector currents.

Base current:

$$\begin{aligned}
I_{be} &= I_{bej}(\exp(P_{be}) - \exp(P_{be0})), I_{bej} = I_{pkc}/\beta_{\max} \\
P_{be} &= (19.347/N_{b1})\cdot\tanh(2 * [(V_{be} - V_j) \\
&\quad + N_{b2}(V_{be} - V_j)^2 + N_{b3}(V_{be} - V_j)^3\cdots]) \\
P_{be0} &= (19.347/N_{b1})\cdot\tanh(2 * [-V_{je} + N_{b2}(-V_j)^2 \\
&\quad + N_{b3}(-V_j)^3 \ldots])
\end{aligned} \tag{8}$$

Collector current:

$$\begin{aligned}
I_c &= I_{cf}\cdot\tanh(\alpha\cdot V_{ce})(1 + \lambda\cdot V_{cb})(5a); \\
I_{cf} &= I_{pkc}(\exp(P_{cf}) - \exp(P_{cf0}))/\cosh(B_{be}(V_{be} - V_{bepm}) \\
P_{cf} &= (19.347/N_{c1})\cdot\tanh(2 * [(V_{be} - V_{bep}) + N_{c2}(V_{be} - V_{bep})^2 + N_{c3}(V_{be} - V_{bep})^3 \ldots]) \\
P_{cf0} &= (19.347/N_{c1})\tanh(2 * [-V_{bep} + N_{be2}(-V_{bep})^2 + N_{bc3}(-V_{bep})^3 \ldots]) \\
\alpha &= \alpha_r + \alpha_s\left(\exp\left(\frac{38.695}{N_{c1}}\cdot V_{ce}\right) - 1\right),
\end{aligned}$$

$$V_{bepm} = V_{bep} + \Delta V_{bep}*(1 + \tanh(P_{cf1}*V_{ce}) - V_{sb2}*(V_{cb} - V_{tr})^2; \tag{9}$$

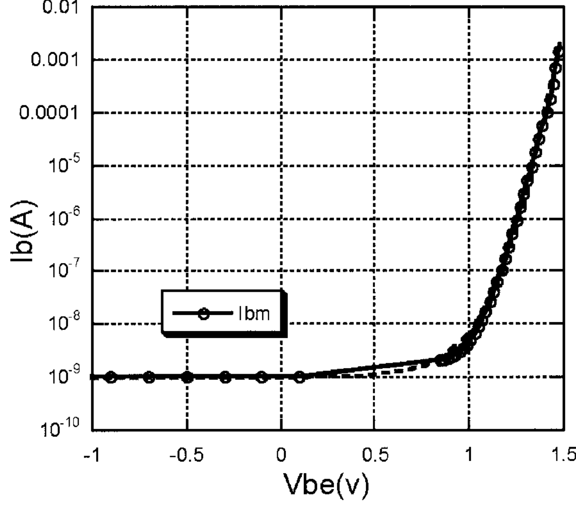

Figure 10. Measured and modeled I_{be}: $I_{je} = 0.00086$, $V_{je} = 1.45$, $P_{be1} = 18.83$, $P_{be1i} = 2$, $P_{be2} = 0$, $P_{be3} = 0$ [see eq. (3b)].

With three terms in the power series model, there are 15 parameters and in single term case we need a total of 11 parameters for the collector and base current: I_{pkc}, V_{bep}, $\beta_{\max}$, B_{be}, N_{c1}, α_r, α_2, λ, N_{b1}, $V_{je} = V_{bep}$, ΔV_{pk}, $I_{bej} = I_{pkc}/\beta\max$.

The base junction current I_{bej} is calculated from $\beta_{\max}$, I_{pkc}; and $V_j \cong V_{bep}$ voltage is taken directly from the measurement. The ideality factor N_{e1} is extracted from the slope of the logarithmic plot. When we define the parameters by using eqs. (8) and (9) we will have correct derivatives, and bounded minimum and maximum currents. This in turn will improve the convergence. This is valid, because the first derivative of tanh is in fact $P_1{*}z$, but it is limited at large deviations as follows:

$$\tanh(P_1 \cdot z) = P_1 \cdot z - (P_1^3 z^3)/3 + (2P_1^5 z^5)/15 \ldots) \quad (9b)$$

Figure 10 shows some measured and simulated results for I_{be}, when the argument is limited by using eq. (8). With one term in the power series, eq. (8) will provide a good fit in many decades.

When using eq. (9), the collector current will be limited from the $\tanh(\alpha \cdot V_{ce})$ for the collector voltage and from the argument for $I_{be} \cong I_{bej} \cdot \exp(19.347 \cdot \tanh(2(V_{be} - V_{je}))$ in the exponential part of I_{be} and I_{ce} versus V_{be}e. This leads to a compact, bounded model with correct derivatives without discontinuities.

III. HBT CAPACITANCES

Devices can operate at high currents and voltages and their nonlinear capacitances need to include both depletion and diffusion parts. The total C_{be} capacitance shows rapid increase and then decrease at high bias. This is also the case for homojunction transistors [7, 14], but for HBTs this increase will be larger than the increase we observe in homojunction transistors. It is a mater of tradition to treat the device capacitance as consisting of two parts — depletion and diffusion — that are connected in parallel.

Diffusion capacitances are described as [1]:

$$C_{bedif} = C_{bep} + C_{be0} \cdot (1 + \tanh[C_{be10} + C_{be11} \cdot V_{be}]),$$
$$C_{bcdif} = C_{bcp} + C_{bc0} \cdot (1 + \tanh[C_{bc20} + C_{bc21} \cdot V_{bc}]). \quad (10)$$

Integrating with the terminal voltages we can obtain the Q_{be} and Q_{bc} when using the following charge definition:

$$Q_{bedif} = C_{be0} \frac{\log[\cosh[C_{be10} + C_{be11} \cdot V_{be}]]}{C_{be11}} + (C_{bep} + C_{be0})V_{be},$$
$$Q_{bcdif} = C_{bc0} \frac{\log[\cosh[C_{bc20} + C_{bc21} \cdot V_{bc}]]}{C_{bc11}} + (C_{bcp} + C_{bc0})V_{bc}. \quad (11)$$

The ordinary equation for the depletion part $C_{dep} = C_{dep0}/(1 - V_{be}/V_{bi})^n$ can create convergence problems when $V_{bc} \geq V_{bi}$. The accepted approach is to define the capacitance with two definitions — below and above V_{bi}. At the connection point, it is important to keep the function and the derivatives equal; otherwise, the HB simulator will not converge. This problem is not easy to solve and can increase the simulation time. For the simulators using charge definitions, some stable solutions, suitable for the capacitance modelling, can be integrated in hypergeometrical functions that are not available in circuit simulators. In addition, the use of such functions will make the extraction difficult. To avoid these problems, the equation for the depletion capacitance equation is modified as follows:

$$C_{dep} = C_{depp} + C_{dep0}(x^2 + m)^{-n-1}(m - (2n - 1)x^2), \quad (12)$$

where $x = V_{bc}/V_{bci}$, n is the grading coefficient, and the m parameter determines the maximum/minimum capacitance ratio where $y = V_{be}/V_{bei}$.

Figure 11 shows comparison between the measurements of the standard depletion capacitance model and the new eq. (12). The model for capacitance C_{bc} can be further extended in $(0 < \boldsymbol{m} < 0.5)$. C_{depp} can

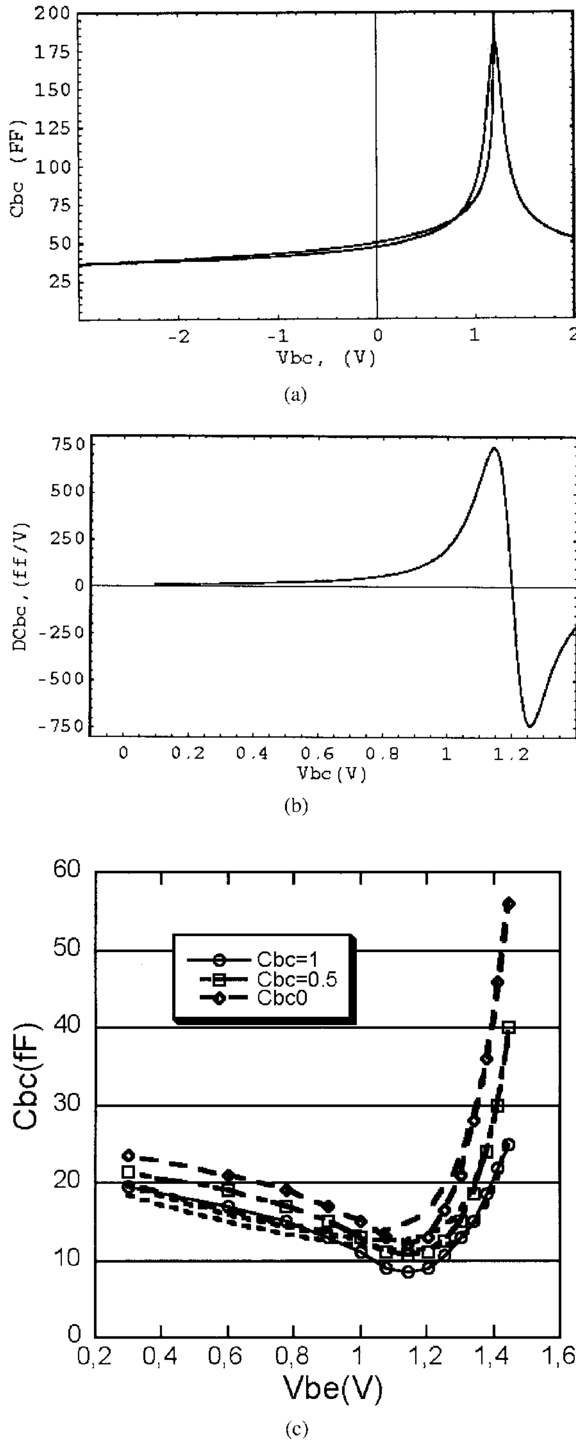

Figure 11. C_{bc} [eq. (12)], $n = 0.3$, $m = 0.002$, $V_{bei} = 1.25$, $C_{dbe0} = 1$; (a) C_{bc} vs. V_{bc}; (b) derivative of C_{bc}; (c) measured and modeled C_{bc} vs. V_{be}.

be associated with the parasitic elements. As is expected, the standard depletion capacitance model has a singularity at V_{bci}. Eq. (12) gives results identical to the textbooks' depletion capacitance definition, but it is well defined at V_{bci} — the function is positive and without poles in the interval $-\infty < V_{bc} + \infty$. The derivatives of the capacitance are also well defined, [see Fig. 11(b)]. In addition, this equation models the decrease of the capacitance as it is in [7, 14] at voltages larger then V_{bci}. This equation can be modified to be completely equivalent to the standard depletion capacitances and used as a direct replacement in the Spice circuit simulators (if required). For the simulators using a charge definition, a simple, closed form of the charge can be derived and combined with the diffusion part [see eq. (11)]:

$$Q_{bcdep} = C_{bcd10}(m + x^2)^{-n}x,$$
$$Q_{bedep} = C_{bed0}(m + y^2)^{-n}y, \qquad (13)$$

where $y = V_{be}/V_{bei}$. The model for capacitance C_{bc} can be further extended in order to consider the dynamic dependence of C_{bc} upon the collector current and an approach similar to that in [5] can be used:

$$C_{bc} \approx C_{dep} * (1 - I_{cf}/I_{cr})^p. \qquad (14)$$

The C_{bc} dependence on the collector current can be transferred directly to the intrinsic voltages by using

$$C_{bc} \approx C_{dep} * \left(1 + \frac{1}{\exp(V_{be} - V_{\min})} + C_{dbe1}\left(\exp\left(\frac{38.695}{N_e}\tanh(V_{be} - V_{\min})\right)\right), \qquad (15)$$

where V_{min} is the voltage (with respective current) at which the capacitance is minimum and C_{dbe1} will determine the slope of the C_{bc} increase at voltages $V_{be} > V_{min}$. This approach corresponds to the device physics and is stable in the extraction, because a limited function, which provides a good fit to the measured C_{bc} [see Fig. 11(c)], is used.

IV. SELF-HEATING MODELING

Figures 12–14 show extracted basic parameters V_{jbe}, P_{be1}, and I_{jbe} at different temperatures. Since the temperature coefficients of different model parameters are small (on the order of 10^{-3}) [8], the changes of the model parameters versus temperature can be considered linear in a limited temperature range [see eq.(16)]. If required, when the temperature range of operation is extended, more terms can be added. The values of I_{ce} and V_{ce} are available from the harmonic balance simulator and are used to calculate both the dissipated power P_{tot} and the junction temperature T_j (calculated dynamically):

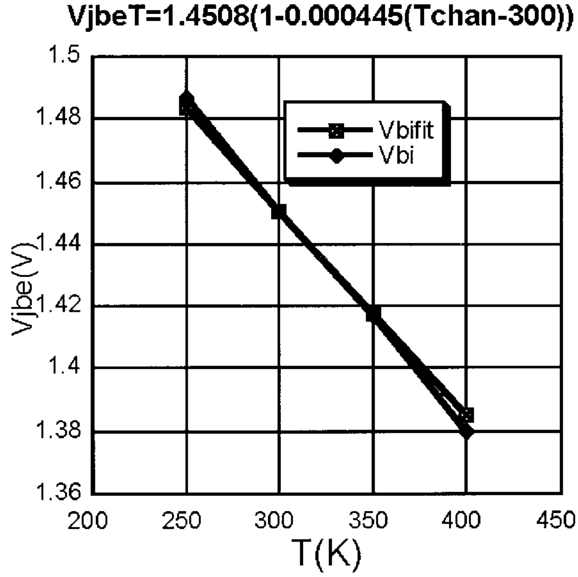

Figure 12. Extracted V_{jbe} vs. T.

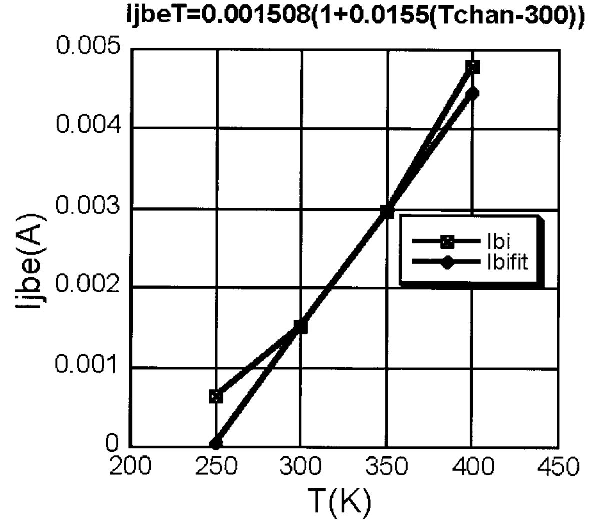

Figure 14. Extracted I_{jbe} vs. T.

$$
\begin{aligned}
P_{tot} &= I_c \cdot V_c + I_b \cdot V_b \\
T_j &= P_{tot} \cdot R_{th} + T_{amb}; \qquad (16)\\
I_{jbeT} &= I_{jbe}(1 + T_{cIjbe}(T_j - T_{ref})), \\
I_{pkcT} &= I_{pkc}(1 + T_{clpc} \cdot (T_j - T_{ref})) \\
P_{beT} &= PP_{be}(1 + T_{cPPbe}(T_j - T_{ref})), \\
V_{jeT} &= V_{jeT}(1 + T_c V_{je} \cdot (T_j - T_{ref})), \\
V_{bepT} &= V_{bep}(1 + T_c V_{bep} \cdot (T_j - T_{ref}))
\end{aligned}
$$

where P_{tot} is the dissipated power and R_{th} is the thermal resistance. For higher accuracy, the thermal resistance R_{th} can be made temperature dependent, that is, R_{thr}.

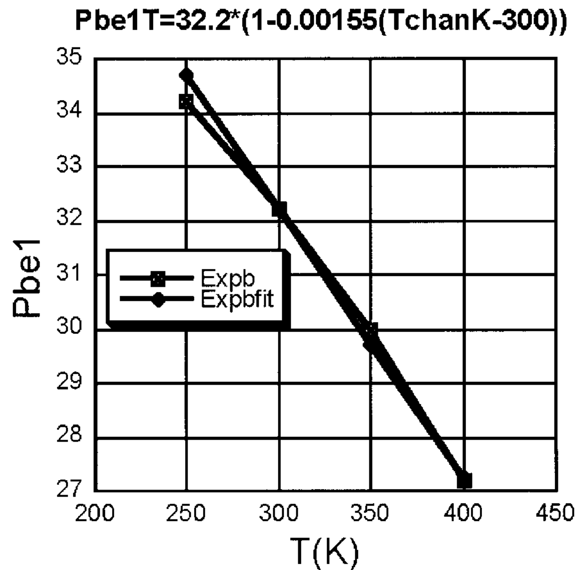

Figure 13. Extracted P_{be} vs. T.

$$
R_{thT} = R_{th}(1 + T_{cRth}(T_j - T_r)) \qquad (17)
$$

Thermal parameters are normalized to the reference temperature T_{ref} at which we extract parameters.

V. BREAKDOWN MODELING

The breakdown is influenced by the effects existing on the base side (with the change of V_{bcp}) and on the collector side. The I_{ce} breakdown can be modeled by using an idea similar to the breakdown model implementation in [33]:

$$
\begin{aligned}
I_{ce} &= I_{pk0} \cdot I_{ef}(1 + \lambda \cdot V_{ce} + L_{sb0} \cdot (V_{cb} - V_{tr})) \\
V_{bcp} &= V_{bep} + \Delta V_{bep} * (1 + \tanh(P_{cf1} * V_{ce} \\
&\quad + KV_{bd2} * V_{cb}) \qquad (18)
\end{aligned}
$$

The value of KV_{bd2} is taking into account the change of intrinsic base voltage V_{bei}, because as a result of this change, the collector current I_{ce} will increase. The coefficient L_{sb0} reflects the sharp increase of I_{ce}, which is influenced by the collector voltage at voltages larger than the threshold V_{tr}, Figure 15.

The breakdown parameters are temperature dependent, and when this problem becomes important, thermal coefficients for the V_{tr}, L_{sb0}, and KV_{bd2} parameters should be extracted.

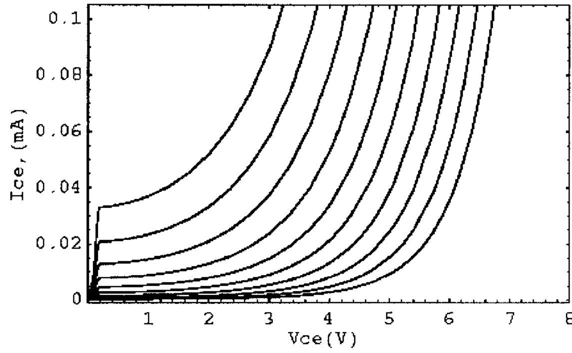

Figure 15. An example of I_{ce} breakdown model using eq. 18: $L_{sb} = 0.1$, $V_{tr} = 1$.

VI. DELAY MODELING

The importance of the proper delay modeling has been very well described in classic papers [5, 13, 26–28]. Figure 16 shows a typical bias dependence of the delay. It increases with the collector current and eventually saturates and decreases, as the collector voltage increases. Usually in the simulators the bias dependence of the delay is defined via I_{ce}, but it can also be defined by directly using the intrinsic controlling voltages and implementing the following equation using CAD:

$$T_{ff} = T_f(1 + 0.5 \cdot Xtf \cdot (1 + \tanh[(38.76/N_e)(V_{be} - V_{je})]) \cdot \exp[V_{bc}/(1.44 \cdot Vtf)]) \quad (19)$$

where T_f is the independent part of the forward delay, Xtf is the bias-dependent part of the forward delay, and Vtf is a fitting coefficient, as they are defined in other software packages such as ADS and ICCAP. In ADS the bias-dependent delay can be implemented using the delay function H of SDD.

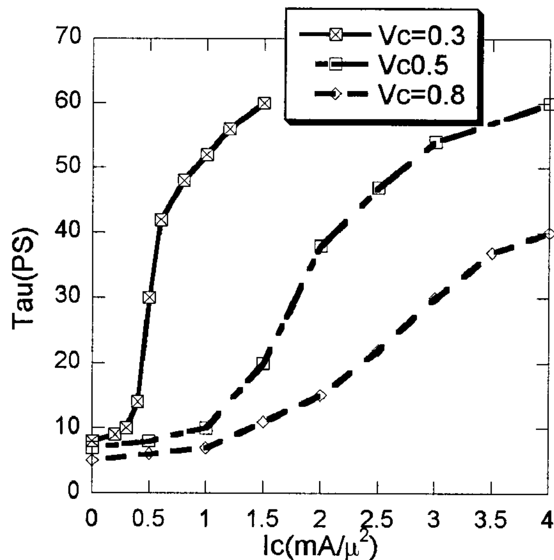

Figure 16. Delay T_{au} vs. Jc density.

VII. EXTRACTION OF THE MODEL

The number of parameters to be extracted using this approach for the nonlinear part of the large signal model is significantly reduced in comparison to other models with comparable accuracy. Many of the model parameters are taken directly from simple measurements. Even when using one term in the power series, the model will be exact at the selected operating point and provide a good global accuracy in 5–6 decades of currents, as shown in Figure 16. When higher accuracy is required (that is, more terms) the remaining fitting parameters can be extracted with simple fitting programs. The reduced number of parameters and the use of bounded functions will result in improved convergence in CAD tools. This is also beneficial for the extraction procedure, because the same problems with convergence are valid for the extraction programs.

The extraction of parameters starts with the extraction of the DC parameters. The basis of the proposed model is that the main parameters are taken directly from the measurements — not extracted. In the simple case of one term in the power series, which is accurate enough for most practical RF applications, the model equations are as follows.

Base current:

$$\begin{aligned} I_{be} &= I_{bej}(\exp(P_{be}) - \exp(P_{be0})), \\ P_{be} &= (19.347/N_{b1}) \cdot \tanh(2 * [(V_{be} - V_{je})]), \\ P_{be0} &= (19.347/N_{b1}) \cdot \tanh(2 * [-V_{je}]). \\ I_{bej} &= I_{pkc}/\beta_{\max} \end{aligned} \quad (8b)$$

Collector current:

$$\begin{aligned} I_c &= I_{cf} \cdot \tanh(\alpha \cdot V_{ce})(1 + \lambda \cdot V_{cb}), \\ I_{cf} &= I_{pkc}(\exp(P_{cf}) - \exp(P_{cf0}))/\cosh(B_{be}(V_{be} - V_{bepm}), \\ P_{cf} &= (19.347/N_{c1}) \cdot \tanh(2 * [(V_{be} - V_{bep})]), \\ P_{cf0} &= (19.347/N_{c1})\tanh(2 * [-V_{bep}]). \end{aligned} \quad (5a)$$

The three base current parameters to be found are: $I_{bej} = I_{pkc}/\beta_{\max}$, N_{b1}, $V_{je} = V_{bep}$. The eight collector currents are: I_{pkc}, B_{be}, V_{bep}, N_{c1}, α_r, α_s, λ, ΔV_{pk}.

I_{bej}, V_{je}, I_{pkc}, V_{bep}, and $\beta_{\max}$ are taken directly from the measurements for currents at which we have maximum β; typically, at $V_k \sim 0.6–0.8$ V. The ideality factors are calculated from the derivative of the I_{be}, which is I_{ce} at this point. The four remaining parameters, B_{be}, α_r, α_s, and λ, can be found with a simple

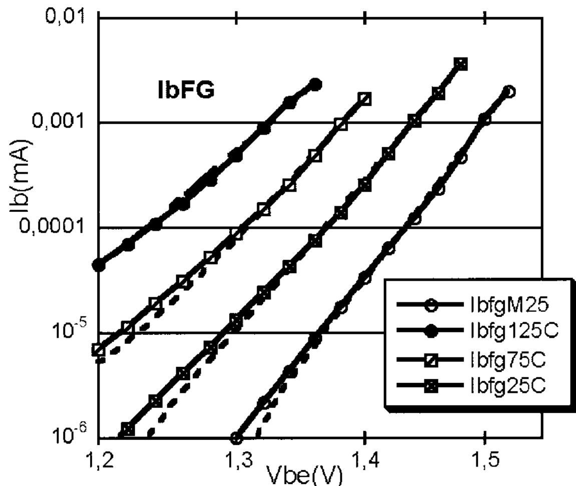

(a)

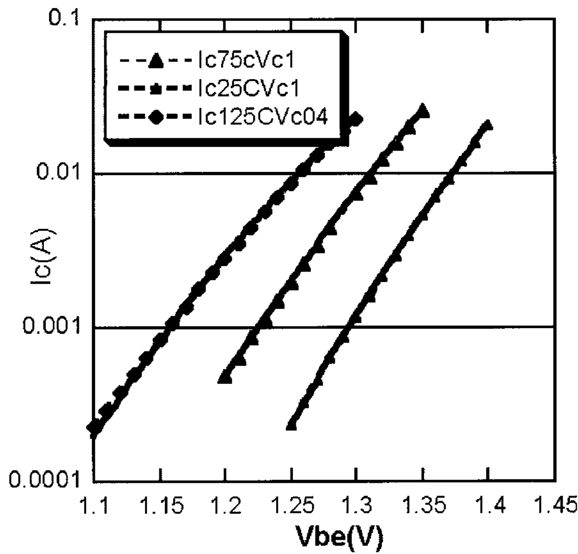

(b)

Figure 17. Measured and modeled I_{be} and I_{ce}: (a) I_{be}; (b) I_{ce}.

fitting program. The parameter B_{be} is found from the β versus V_{be} dependence, parameter α_r will influence I_{ce} at small currents, and low $V_{ce} < V_k$ and α_s parameters will influence the shape of I_{ce} at the knee V_k. The output conductance parameter λ will fit the I_{ce} at voltages above V_k and this give the possibility to fit α_r, α_s, and λ separately.

There are many fitting programs such as Mathematica, MathCAD, Kaleidagraph, XLfit3, and so forth that can be used to fit basic parameters of the model. Figure 17 shows some results from measured and modeled I_{be}, I_{ce} (measured points and modeled lines) with one term in the equations using a simple fitting program (Kaleidagraph), and if more terms are used in the power series in the argument. In addition, we can use specialized extraction programs such as ICCAP.

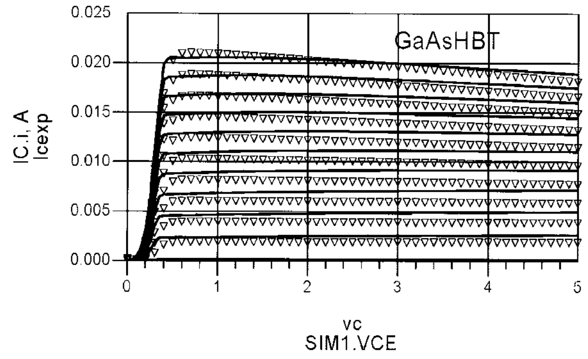

Figure 18. I_{ce}: I_{be} = 20–200 μA step 20 μA.

The peak current $I_{cmax} \approx I_{ce}$ is close to the currents for which we have maximum β with corresponding V_{ce}. P_{cf1} can be extracted directly from the derivative of the argument (ideality factor) at the selected bias voltage V_{be} (see Fig. 8), such that $P_{cf1} = g_m/I_{cmax} = 38.695/N_{c1}$. A typical value for the extracted base current is $I_{ib} \approx 0.2$–2 mA with the corresponding V_{be}.

There is a large amount of papers on the extraction of parasitics in the small-signal equivalent circuit [8, 14–28] of HBTs. Some of the parasitics such as the resistances and capacitances used in this study are available directly from measured data. The R_e extraction was compared using both the open-collector method and the high-frequency extraction method proposed by S. Maas [18]. The rest of the parasitics are found from optimization by using the CAD tool set for multiple-bias S-parameter optimizations.

Generally, the base resistance R_b in these types of transistors is rather low (this is one of their benefits) and, in order to simplify the model extraction, the base and collector resistances in this case were considered constant. The base resistance consists of three parts as follows: $R_b = r_b + r_{bs} + r_{b0}$, where r_b is active, r_{bs} is spreading resistance, and r_{b0} is ohmic metal contact resistance. The series-access components are bias independent and when the injection level

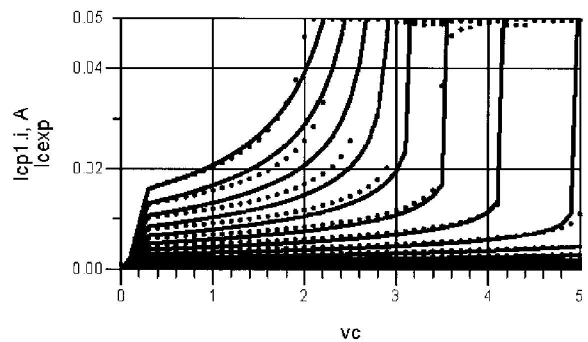

Figure 19. I_{ce}, $V_{be} > 1.2$–1.4 V.

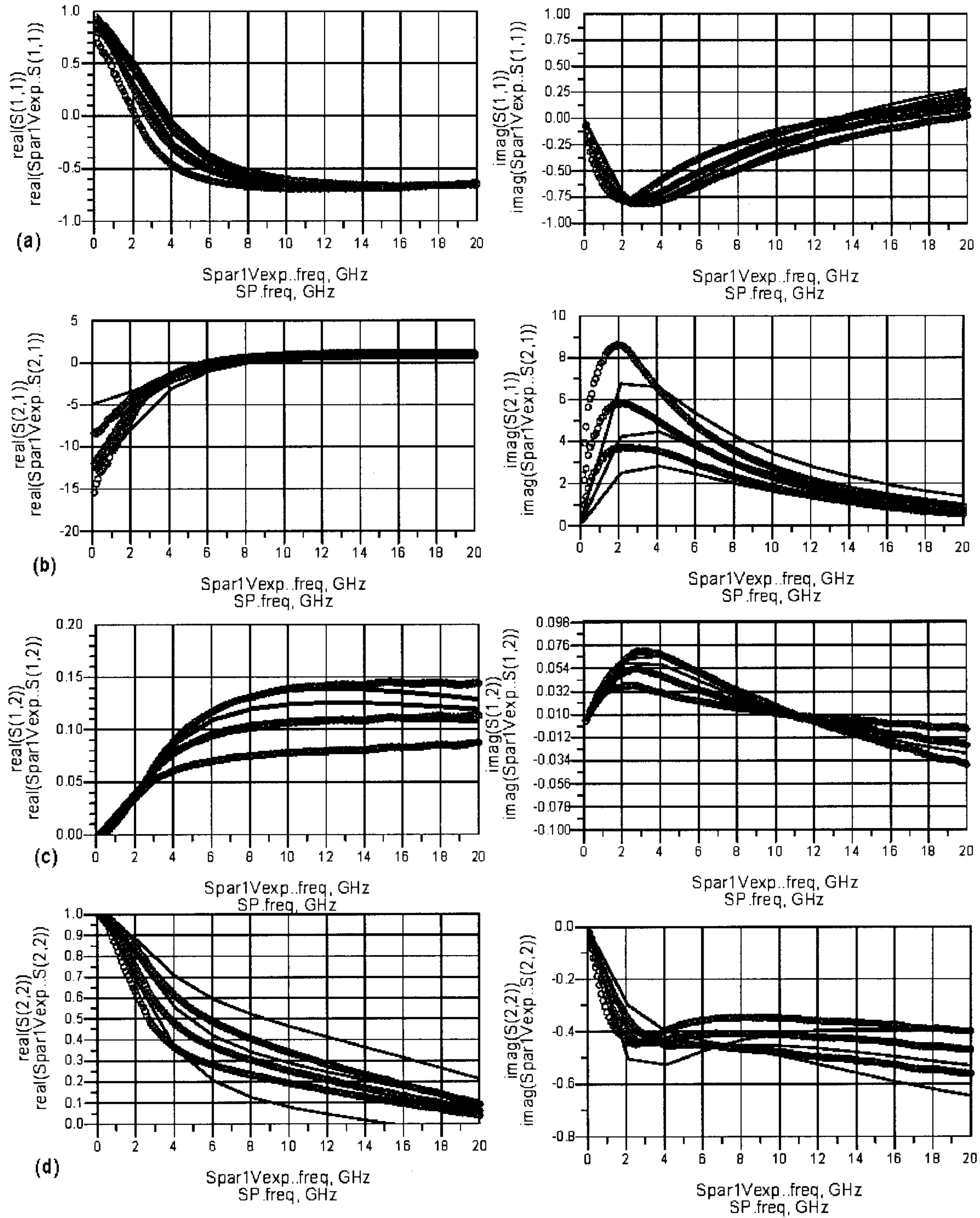

Figure 20. Measured and modeled magnitude and phase S_{11}, S_{21}, S_{12}, S_{22}, V_{ce} = 3 V; V_{be} = 1.32, 1.34, and 1.36 V.

is high, the changes of R_b are very small and can be neglected. If required, the bias dependence of R_b can be modeled using approach similar to that in [6, 34]:

$$R_b = \frac{R_{b\,\max}}{1 + (I_b/I_{b0})^{arb}} \qquad (20)$$

VIII. EVALUATION OF THE MODEL

The model was implemented as an SDD in MDS and ADS (Agilent) with self-heating and delay, and was experimentally evaluated using DC, *S*-parameter and power-spectrum measurements.

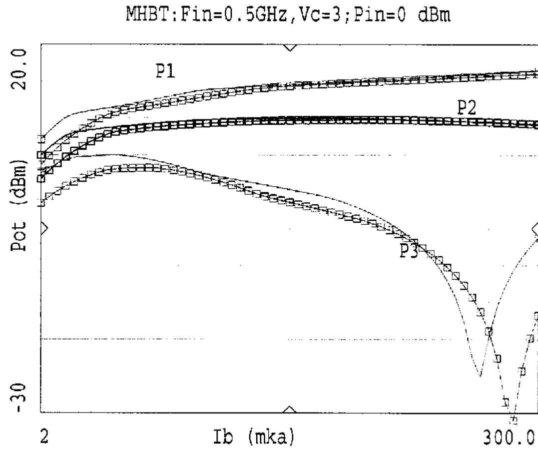

Figure 21. Measured and modeled PS, $V_{ce} = 3$ V, I_b: 2 to 300 μA.

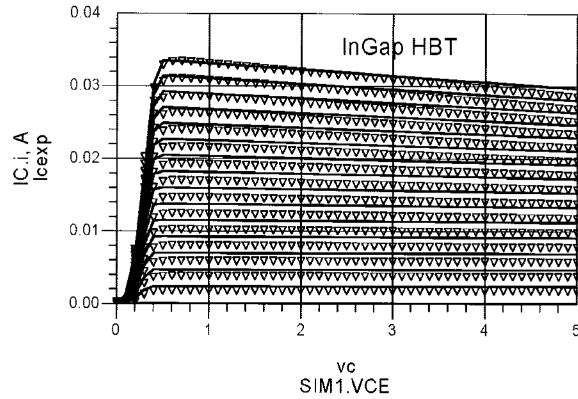

Figure 23. Measured and modeled I_{ce} for InGaP HBT, I_{be}: 2 to 300 μA.

Figures 18 and 19 show measured and modeled I_{ce}. In the example shown in Figure 18, the base current I_{be} is a parameter and in Figure 19, V_{be} is a parameter. The fit is good, even with such a simple definition of the model and using two terms in the power series for I_{ce}. Despite this simplicity, the model is able to describe the thermal runaway of Figure 19, with an accuracy similar to more complicated models in the practical range of currents and voltages with a significantly reduced number of parameters.

Figure 20 shows some results of S-parameter measurements and simulations. The model accurately describes the small-signal behavior.

The large-signal properties of the model were evaluated using a PS method [31]. Figures 21 and 22 show some results of the measurements and simulations, and the fit is good. The models for currents and capacitances facilitate the convergence in large-signal applications, due to the use of well-defined functions and symmetry.

The model definitions are quite general and can be applied to other types of HBT, as well as ordinary Si bipolar transistors. Figure 23 shows the results of the measured and simulated I_{ce} for InGaP HBT.

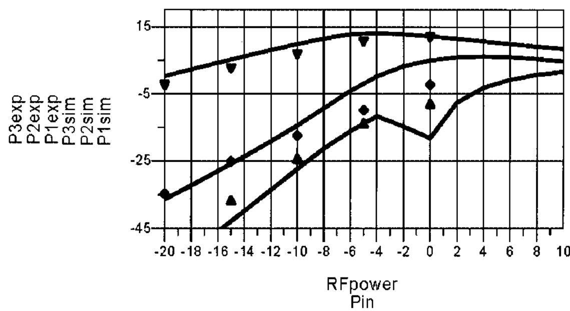

Figure 22. Measured and modeled PS, at 5 GHz, $I_{be} = 0.25$ mA, $V_{ce} = 2$ V.

Figures 24 and 25 show measured and modeled I_{be} and I_{ce} for a commercial Si microwave transistor AT 42070 (Agilent). With one term in the power series, the fit is very good for the practical range of currents.

This approach can be extended with more features, which we will eventually need in order to model more complicated effects in HBTs and BJTs. For example, the bias dependence of the output conductance in certain HBTs and high-power Si BJTs can be strongly bias dependent and, in order to track this, the output conductance parameter λ can be made bias dependent:

$$I_c = I_{cf} \cdot \tanh(\alpha \cdot V_{ce})(1 + \lambda * V_{cb} + \lambda_{\max}) \quad (21)$$

$$\lambda_{\max} = \lambda_2 * V_{cb} * \left(1 + \tanh\left(\frac{19{,}347}{N_{cf}} * (2(V_{be} - V_{bep}))\right)\right) + \lambda_3/(1 + V_{ce}^2) \quad (22)$$

In this case, the additional term λ_2 provides dependence of the output conductance on the base voltage V_{be} and λ_3 on collector voltage V_{ce}. The parameter λ_2 is effective at high V_{ce} and λ_3 at low V_{ce}. Even in this case of complicated output conductance, the number of extracted parameters (11) is rather small, the model is stable in extraction & simulations, because functions used in the model are monotonic and limited.

Figure 26 shows some results modeling SiGe HBT and high-power Si BJT is shown in Figure 27. The correspondence between the measured parameters and model is good, even using one term in the power series. In these examples of a complex output-conductance dependence, the total number of I_{ce} and I_{be}

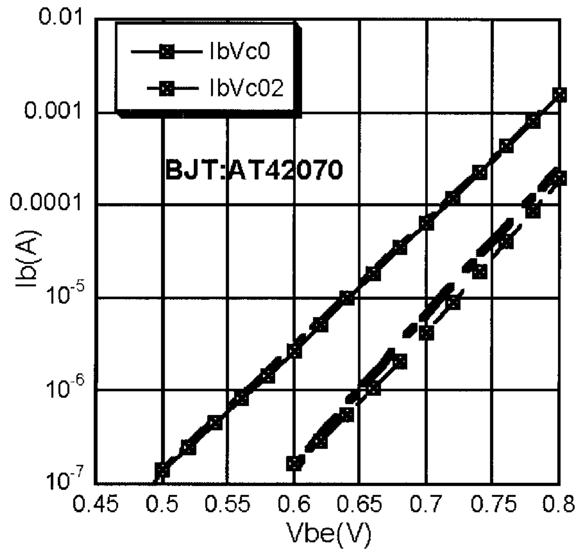

(a)

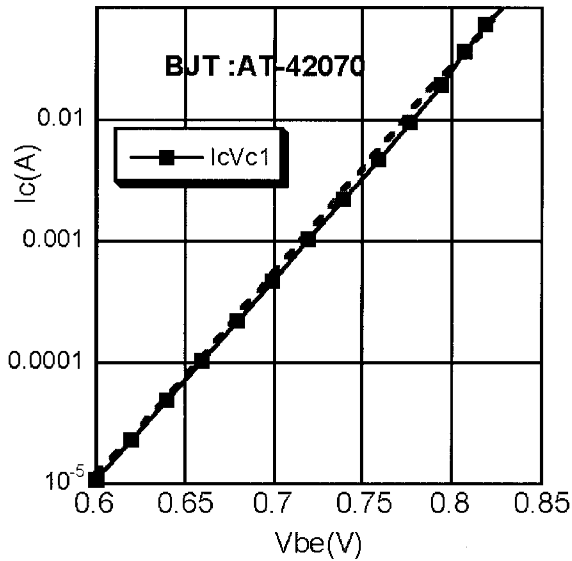

(b)

Figure 24. Measured and modeled (a) I_{be} and (b) I_{ce} for I_{ce}, AT42070 BJT.

current parameters is 11, with one term in the power series; however, this is sufficient to provide good accuracy in the practical working range of currents and voltages. If for some reason a higher global accuracy is required, then two more terms can be added to the power series in the argument.

IX. CONCLUSION

A simple bias-dependent HBT model applicable to CAD was proposed and implemented. The model was experimentally evaluated using DC, *S*-parameter, and power-spectrum measurements, and good correspondence was obtained between the measurements and the model. The model can be adopted for use as a simple BJT model.

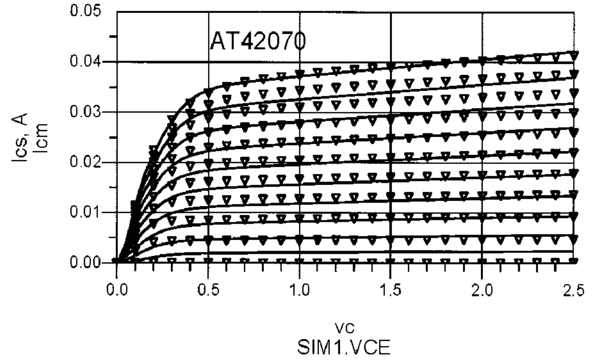

Figure 25. ADS implementation—measured and modeled results for I_{ce}, AT42070, I_{be}: 1–400 μA $I_{pkc} = 58$ mA, Vbep = 0.77, $Pcf1e = 14$, $Pcf1i = 3$, $Ijbe = 0.41$ mA, $V_{jbe} = 0.76$, $P_{be1e} = 16.5$, $P_{be1i} = 2$, $\alpha_\tau = 0.5$, $\alpha_s = 8$, $\lambda \ominus 0.09$.

ACKNOWLEDGMENT

The authors wish to acknowledge Agilent for the donation of high-frequency simulation software, S. Maas for valuable discussions, and H. Zirath, E. Kollberg, A. Olaussen, and SSF for their help and support.

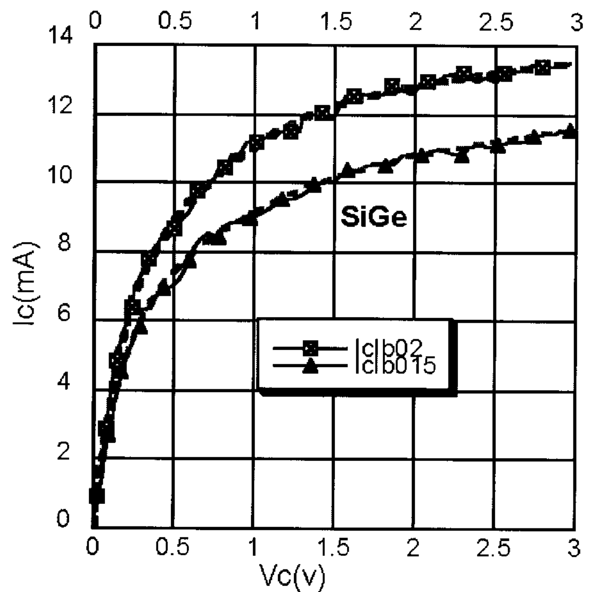

Figure 26. Measured and modeled results for I_{ce}, SiGe HBT.

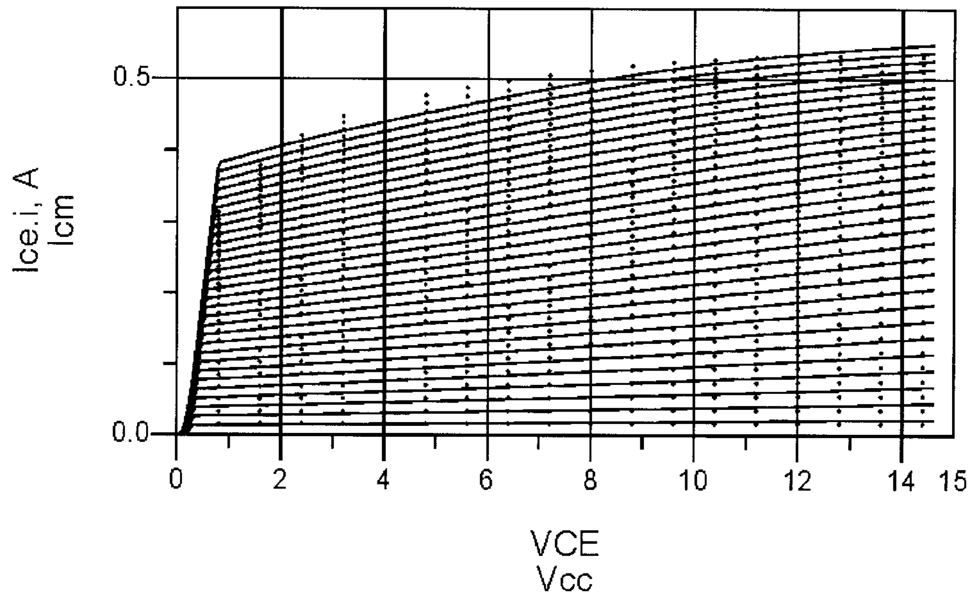

Figure 27. Measured and modeled results for I_{ce}, BC141.

REFERENCES

1. P.C. Grossman and J. Choma, Jr. Large-signal modelling of HBT including self-heating and transit time effects, IEEE Trans MTT 40 (1992), 449–464.
2. C. Colin, J. Seitchik, D. Bowers, M. Dunn, J. Getreu, M. Swain, S. Moinian, J. Parker, M. Schroter, and L. Wagner, VBIC95: The vertical bipolar inter-company model, IEEE J SSC 31 (1996), 1475–1483.
3. R. Anholt, Electrical and thermal characterization of MESFETs HEMTs, and HBTs, Artech House, Boston, 1995.
4. K. Lu, P. Perry, and T. Brazil, A new large-signal AlGaAs/GaAs HBT model including self-heating effects, with corresponding parameter extraction procedure, IEEE Trans MTT 43 (1995), 1433–1445.
5. L. Camnitz, S. Kofol, T. Low, and R. Bahl, An accurate large signal high frequency model for GaAs HBT, GaAs IC Symp, 1996, pp. 303–306.
6. UCSD Model, UCSD Electrical and Computer Engineering Dept., 1995
7. S. Tiwari and D. Frank, Analyses of the operation of GaAlAs/GaAs HBTs, IEEE Trans ED 36 (1989), 2105.
8. C. Wei, C.M. Hwang, W. Ho, and J. Higgins, Large signal modelling of self-heating, collector transit time and RF breakdown effects in power HBTs, IEEE Trans MTT 44 (1996), 2641.
9. Rudolph, R. Doerner, and P. Heymann, New GaInP/GaAs-HBT large-signal model for power applications, EUMC'98, 1998, p. 231.
10. K. Gummel and H.C. Poon, An integral charge control model of bipolar transistors, BSTJ 49 (1970), 827–852.
11. G.M. Kull, L. Nagel, S. Lee, P. Lloyd, J. Prendergast, and H. Dirks, IEEE Trans ED ED 32 (1985), 1103–1113.
12. J. Fossum, Modelling issues for advanced bipolar device/circuit simulations, Bip Trans Mtgs (1989), 234–241.
13. J. Scott, Nonlinear III-V HBT compact models: Do we have what we need? IEEE MTTS Digest, 2001, 663–666.
14. S. Laux, Technique for small-signal analysis of semiconductor devices, IEEE Trans ED 32 (1985), 2028–2037.
15. K. Joardar, A new technique for measuring junction capacitance in bipolar transistors, IEEE Bipolar/BiCMOS Circuits Technol Mtg, 1995, p. 133.
16. H.C. Poon and H.K. Gummel, Modelling of emitter capacitance, Proc IEEE (1969), 2181.
17. R. Anholt, J. Gerber, R. Tayrany, and J. Pence, HBT model extractor for spice and harmonic balance simulations IEEE MTT-S (1994), 1257.
18. S. Maas and D. Tait, Parameter-extraction method for heterojunction bipolar transistors, IEEE Microwave Guided Wave Lett 2 (1992), 502–504.
19. D. Pehlke and D. Pavlidis, Evaluation of the factors determining HBT high frequency performance by direct analysis of S-parameter Data, IEEE Trans MTT 40 (1992), 2367–2373.
20. D. Dawson and A. Gupta, CW measurement of HBT thermal resistance, IEEE Trans ED 39 (1992), 2235.
21. W.J. Klosterman, J. Paasschens, and D. Klaassen, Improved extraction of base and emitter resistance from small signal high frequency admittance measurements, IEEE BCTM (1999), 93–96.
22. HBT Static Model IC-Cap Users' Meeting, 1996.
23. D. Costa, W. Liu, and J. Harris, Direct extraction of the AlGaAs/GaAs heterojunction bipolar transistor small-signal equivalent circuit, IEEE Trans ED 38 (1991), 2018–2024.

24. P. Baureis and D. Seitzer, Parameter extraction for HBT's temperature-dependent large-signal equivalent circuit model, IEEE GaAs IC Symp, 1993, 263–267.
25. Y. Suh, D. Heo, A. Raghavan, E. Gebara, S. Nuttnick, K. Lim, and J. Laskar, Direct extraction and modelling method for temperature-dependent large-signal CAD model of Si-BJT, MTTS-Dig, 2001, pp. 971–974.
26. M. Schröter and T. Lee, Physics-based minority charge and transit time modelling for bipolar transistors, IEEE Trans ED 46 (1999), 75.
27. D. Teeter and W. Curtice, Comparison of hybrid pi and tee HBT circuit topologies and their relationship to large-signal modelling, MTTS-Dig, 1997, pp. 375–378.
28. M. Rudolph, R. Doerner, K. Bilenhoff, and P. Haymann, Unified model for collector charge in heterojunction bipolar transistors, IEEE Trans MTT 50 (2002), 1747–1751.
29. M. Rudolph, F. Lenk, R. Doerner, and P. Haymann, On the implementation of transit-time effects in compact HBT large-signal models, MTTS-Dig, 2002, pp. 997–1000.
30. T. Shimura, T. Miura, Y. Uneme, H. Nakano, R. Hattory, M. Otsubo, K. Mori, A. Inoue, and N. Tanino, High efficiency AlGaAs/GaAs power HBTs at a low supply voltage for digital cellular phones, IEICE Trans Electron E80-C (1997), 740–745.
31. L. Bengtsson, C. Hedenas, and I. Angelov, Verification of an HBT Gummel–Poon model by power spectrum, EUMC 1996, 911.
32. I. Angelov, K. Choumei, and A. Inoue. An empirical HBT large-signal model for CAD, 2002 MTTS-Dig, 2137–2140.
33. Microwave Office, Element catalogue, 2002.
34. M. Linder, F. Ingvarsson, K. Jeppson, and J. Grahn, Extraction of emitter and base series resistances of bipolar transistors from a single dc measurement, IEEE Trans Semiconductor Manufacturing 13 (2000), 119–125.

BIOGRAPHIES

Iltcho Angelov was born in Bulgaria. He received an M.Sc. degree in electronics (1969) and a Ph.D. in mathematics and physics from Moscow State University (1973). From 1969–1991 he was with Institute of Electronics, Bulgarian Academy of Sciences, Sofia, as a Researcher, Research Professor (1982), and Head of the Department of Microwave Solid State Devices (1982). Since 1991 he has been with Chalmers University, Göteborg, Sweden and is a member of IEEE . His main interests are in device modelling and low noise and nonlinear circuit design.

Kenichiro Choumei was born in Osaka, Japan in 1968. He received B.S. and M.S. degrees in electronics engineering from Doshisha University, Japan, in 1992 and 1994, respectively. Since joining the Optoelectronic & Microwave Devices Laboratory, Mitsubishi Electric Corporation, Itami, Japan, in 1994, he has been engaged in the research and characterization of various GaAs power devices for mobile communications. He also developed microwave measurement systems. His present research interests include characterization and device modeling of HBT as well as circuit design of millimeter-wave MMICs and their modules, such as HBT-based and HFET-based VCOs. He is a member of the IEEE and the Institute of Electronics, Information and Communication Engineers of Japan (IEICE).

Akira Inoue was born in Osaka, Japan in 1961. He received B.S. and M.S. degrees in physics from the University of Kyoto, Japan, in 1984 and 1986, respectively. In 1986 he joined the LSI Laboratory, Mitsubishi Electric Corporation, where he was engaged in the design of GaAs MMIC. In 1988 he joined the Optoelectronic & Microwave Devices Laboratory, where he participated in the characterization of GaAs transistors, evaluation, and the design of modules and MMICs. He developed microwave measurement such as on-wafer RF testers, harmonic load-pull system, and microwave waveform measurement. Currently, he has been engaged in the development of microwave power transistors and power amplifier modules for mobile communications. He has developed inverse class-F power amplifiers for mobile handsets. He is also working on the developments of GaAs FET and HBT modeling. He is a member of the IEEE and the Institute of Electronics, Information and Communication Engineers of Japan (IEICE).